Compact Magnetron Power Supply for Industrial Heating Applications

Shansong Wei[1], Alan J. Watson[1], Rishad Ahmed[1], and Jon Clare[1]
[1] University of Nottingham, UK

***Abstract*-- This paper proposes a 100 kHz Silicon, Carbide based, 8.1 kW magnetron power supply for industrial heating applications. Operation at this high frequency along with transformer optimization results in a smaller physical footprint, which is advantageous in some heating applications, such as those undertaken offshore. Simulation work using an electrical model for the Magnetron is used to demonstrate the effectiveness of the control methodology presented and the experimental verification is ongoing. This power supply can also be scaled up for use in magnetrons over 100 kW.**

***Index Terms*— Modulators, High Voltage, Transformer Design, RF Power**

I. Introduction

Recently, there has been an increasing concern about the environmental pollution resulting from the burning of fossil fuels for heating applications [1]. To respond to this there has been an increase in the demand for the electrification of some heating applications. This has accelerated the growth in the demand for using electrical power to replace the conventional fuels for industrial heating systems and this trend has no sign of slowing [2]. Microwave-based (RF) approaches to heating have been of interest since the development of the first Magnetron by the researchers at the University of Birmingham in 1940 [3]. The RF generation components in the microwave-based systems include a Magnetron and the drive of such a device is the subject of this paper.

Microwave-based systems using Magnetrons can be applied to food processing, mining, material treating and many other applications [4]. One of the scenarios previously studied is the oil treatment of waste material from offshore drilling rigs. Traditional methods for cleaning oil from this waste involve high-risk craning activities. The risks can be significantly reduced by treating the waste material offshore using Microwave energy. However, due to the platform area limitations, a small size for the required hardware is critical for use on offshore rigs [5]. Traditional low frequency approaches to generate the required voltage for the operation and control of a Magnetron tube occupy significant space. This physical footprint can be reduced by operating at higher frequencies. Recent advances in drive systems for high power Magnetron devices have been based on resonant converters operating under 25 kHz using silicon IGBT switches [6] [7]. The use of a resonant circuit and its potential for facilitating soft switching in the power switching devices is well known [8]. However, the presence of the resonant tank also can significantly complicate the control of these converters. To meet the future demand for the advanced RF-based industrial processing systems, more tailored and improved electrical power supplies need to be developed. To increase the power density, as previously stated as the requirement, new approaches, enabled by recent advances in switching device technology, are required.

One way to reduce the converter size and weight is to increase the switching frequency of the converter. This has been limited by the available affordable semiconductor technologies over the past few decades – the efficiency of hard switched silicon IGBT based converters reduce dramatically at high frequency. Even with soft switching designs, the maximum operating frequency is still relatively low. With the recent development in wide bandgap semiconductors, and in particular, commercially available silicon carbide (SiC) MOSFETs the potential for operating at the higher switching frequency, efficiently, has been enabled.

In this paper, a SiC MOSFET based single active bridge (SAB) circuit is proposed to drive a magnetron with a peak RF power of 6 kW. As a result of the efficiency of the Magnetron device, a power supply capable of producing 7.2 kV to 7.5 kV at up to 1.08 A is required. The nature of the Magnetron load also requires a combined voltage and current approach for the SAB circuit. Hence, the circuit modelling and control strategies for both current and voltage modes are carried out and presented. A Magnetron electrical emulator has been developed to provide an accurate load for the simulation work presented. Currently, only limited literature mentions high frequency transformer designs at this voltage and power level [9] [10]. As a result, an optimisation approach to the design for this application is described and used to derive key characteristics for the required transformer.

II. Magnetron Emulator

An illustrative diagram of the electrical characteristic of the 6 kW Magnetron is shown in Fig. 1 for operation at a particular magnetic flux density. Before the anode voltage reaches the knee voltage, the Magnetron is not operating and has a very large resistance. After the anode voltage passes this knee in the characteristic, the Magnetron starts to output the microwave energy which can be used for industrial heating and the load resistance apparent at the converter output terminals reduces dramatically. This

resistance is known as the slope resistance (R_{slope}). The anode current becomes very sensitive to the change in anode voltage under this condition. With a fixed knee voltage, the output microwave power can be controlled by varying the anode current.

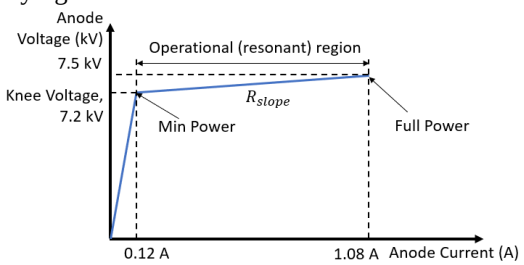

Fig. 1: Target Magnetron V-I characteristics

Due to the non-linearity of the Magnetron load, a simple resistor cannot fully represent its load characteristics. An approach to the modelling of the Magnetron uses two modes: the first before and the second after the anode voltage reaches the knee in the characteristic. As Fig. 1 shows, under the first condition, the Magnetron can be modelled as R_1. For the second one, it can be modelled as R_{slope}. Based on the voltage and current shown above, R_1 and R_{slope} can be calculated to $60\,k\Omega$ and $312.5\,\Omega$, respectively [11]. An emulator circuit is designed based on these characteristics, as shown below. The parallel resistance of R_1 and R_2 equals to R_{slope}. When the knee voltage is not reached, only R_1will conduct. After the output voltage passes V_{knee}, both R_1 and R_2 conduct to ensure the correct load resistance for this operational level of the RF tube. The diode in Fig. 2 can guarantee that the resistors are conducting in the designed way. The output current is measured before both resistors so that under all circumstances the measurement is correct.

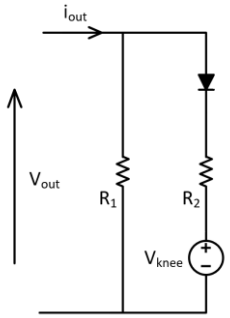

Fig. 2: Magnetron emulator circuit

III. Proposed Converter for High Power Industrial Magnetron

A. Converter structure

Due to the switching loss restrictions of the Silicon based IGBT switches, operation at higher switching frequencies in magnetron power supplies has only really been achieved by using resonant converter technologies [7]. However, the problems with the resonant converter such as complicated control on low power operation and sensitivity to circuit parasitic components make it unfavourable for state of art designs. The SiC MOSFETs, on the other hand, enabled efficient high switching frequency converter designs without the need for a resonant tank.

Although there are many applicable DC-DC converter topologies, considering the power level, a full-bridge based converter is the most likely structure [12]. In such applications, it is preferred to avoid the use of a filter inductor on the output stage connected to Magnetron. This is because it must be designed as a high voltage component but may also result in Magnetron stress under fault conditions in the Magnetron tube [13]. If there is a fault in the Magnetron, resulting in an open circuit, the best way to protect the RF tube is to shut down the converter so that no more energy will be supplied into the RF tube (resulting in a high voltage). With a DC side inductor, under such conditions, the stored energy in the inductor may be transferred to the output filter capacitor of the converter, potentially resulting in a high voltage being presented to the Magnetron, reducing its lifetime. Some existing solutions for this application use a voltage multiplier on the output stage to boost up the voltage. However, it is not adopted in this case since it results in excessive ripple current. This will lower the quality of the RF produced and distort its power spectrum [14]. Removing this ripple requires larger filter capacitors on the output of the converter, which is only really feasible on lower voltage tubes, for example under 5 kV, since wider component choices are available, as previously reported [15] [16].

Fig. 3 shows the schematic of the proposed converter. The SAB idea was first proposed in 2001 by G. D. Demetriades for high-power step-down applications, with a half-bridge on the primary side. With appropriate snubber capacitors, the converter is capable of soft turn on [17]. In the case of this work, an H-bridge is connected to a fixed DC voltage source. The output square wave voltages are filtered by the inductor in the ac link of the primary side, before reaching the high-frequency transformer, which steps up the voltage to the required level for the magnetron. The inductor current is rectified, before being filtered by the output capacitor. Finally, the required voltage and current are delivered to the Magnetron load which is connected in parallel with the output filter. A 3-phase interleaved version of this converter is adopted for this work due to the high output current and power. Furthermore, interleaving reduces the output current ripple, which leads to smaller filter capacitors at the output side. One phase of the three-phase circuit is analysed here for brevity.

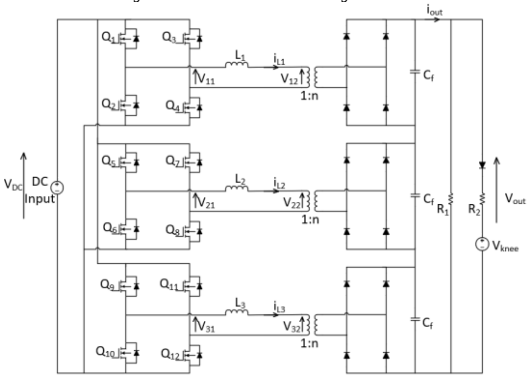

Fig. 3: 3-phase interleaved SAB converter circuit for high power industrial Magnetron

Where in phase 1, V_{11} and V_{12} are the H-bridge and transformer primary voltage; i_{L1} is the current of the inductor L_1 and C_f is the filter capacitor at the output side. The labels for the other two phases are similar to phase 1.

B. Converter modelling and validation

The SAB circuit can operate under both continuous conduction mode (CCM) and discontinues conduction mode (DCM). Since the operation is different under the two modes, the transfer functions should be derived separately. For the Magnetron type of load, as explained in the previous section, it would not start to produce microwave energy before the knee voltage is reached, and a voltage controller is therefore necessary. After the Magnetron starts to conduct, a current controller is needed to precisely control the output current (ripple in the tube current will result in a lower quality in the RF produced). Hence, the converter needs to be modelled for both current and voltage modes.

The main converter voltage and current components are labelled in Fig. 3. The duty cycle, d, is measured over a half period. The corresponding key current and voltage waveforms are presented in Fig. 4 and the converter behaviours are shown in Fig. 6 and Fig. 7.

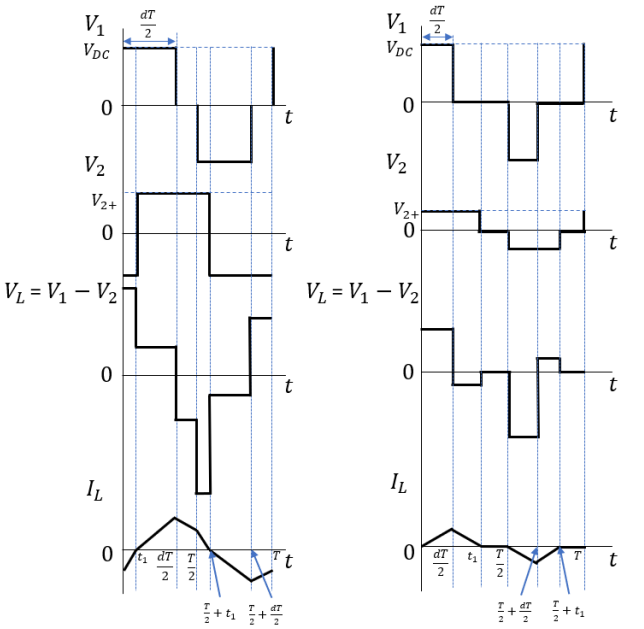

Fig. 4: Current and voltage waveforms under CCM (left) and DCM (right) mode

The equivalent circuit for the SAB converter is shown in Fig. 5 with all the components referred to the primary side.

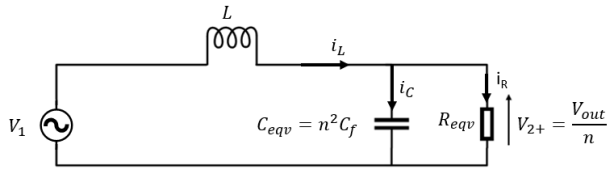

Fig. 5: SAB equivalent circuit referred to the transformer primary side

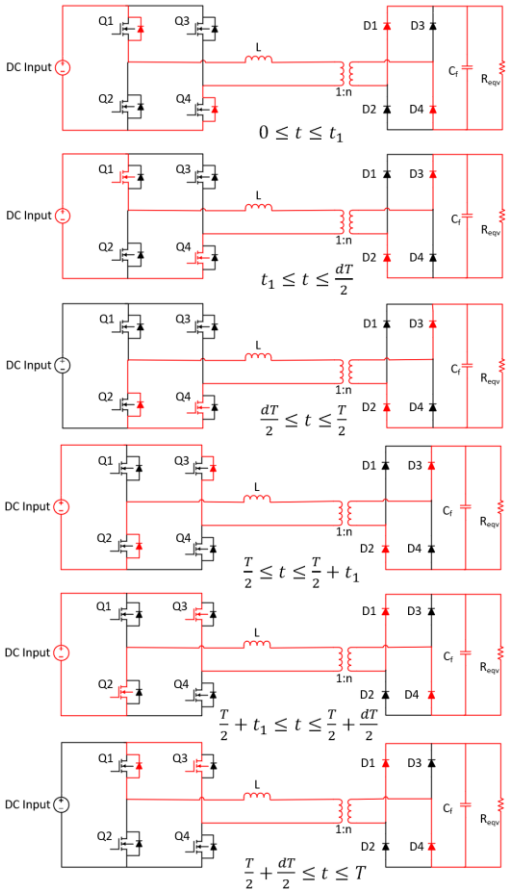

Fig. 6: Converter behaviour under CCM

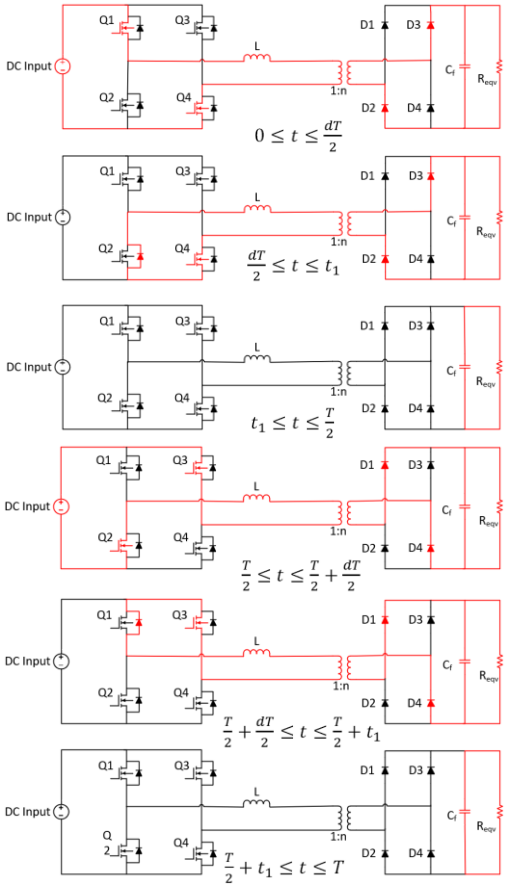

Fig. 7: Converter behaviour under DCM

Here the R_{eqv} is the load resistance referred to the primary side. Its value before and after the Magnetron starts to produce RF power, are expressed in equations 1 and 2 respectively.

$$R_{eqv} = \frac{R_1}{n^2} \quad (1)$$

$$R_{eqv} = \frac{R_{slope}}{n^2} \quad (2)$$

As the output current I_o is the inductor mean absolute current $\overline{|i_L|}$ scaled by the transformer turns ratio n, the circuit could be modelled by a $\overline{|i_L|}$ to d transfer function. The CCM transfer function is found to be

$$\frac{\widetilde{\overline{|i_L|}}}{\tilde{d}} = \frac{(1-d_0)V_{DC}T}{4L} \quad (3)$$

and the DCM transfer function is found to be

$$\frac{\widetilde{\overline{|i_L|}}}{\tilde{d}} = \frac{V_{DC}(V_{DC}-V_2)d_0T}{2V_2L} \quad (4)$$

where d_0 is the nominal operation point for linearization. Since the output voltage control is only used during start-up, which is under DCM mode, the output voltage transfer function for DCM can be derived as

$$\frac{\widetilde{v_{out}}}{\tilde{d}} = \frac{\frac{2V_{out}}{D}}{sCR+2+\frac{M}{1-M}} \quad (5)$$

Where

$$M = \frac{\frac{V_{out}}{n}}{V_{DC}} \quad (6)$$

It should be noted that the load resistance for the current transfer functions is R_{slope} while it is R_1 for the voltage transfer function, to represent the significant drop in load after the Magnetron starts to generate RF power. It can be observed that the current transfer functions for both CCM and DCM modes are quite similar. The reason is the inductor current resets to zero after each cycle for both conditions and there is no resonance between the inductor and capacitor during operation.

The designed components values are shown in Table 1, based on one phase of the 3-phase interleaved modules. All phases have the same component values. These are designed to ensure that minimum energy is stored in the converter whilst still meeting the required output voltage ripple requirement of 2%.

Table 1: Circuit parameters

Input voltage, V_{DC}	750 V	Duty cycle at full power, d	0.6
Output voltage, V_{out}	2.5 kV	Transformer turns ratio, n	1:6
Output current, I_{out}	1.08 A	Primary side inductance, L	76.9 µH
Switching frequency, f	100 kHz	Output capacitance, C	20 nF

The $\overline{|i_L|}$ to d transfer functions, are a simple gain and are found to be

$$G_{ICCM} = 9.7562 \quad (7)$$

$$G_{IDCM} = 16.4067 \quad (8)$$

Where the transfer functions are linearized at $d_0 = 0.6$ and $d_0 = 0.4$ for CCM and DCM modes, respectively. After linearizing at $d_0 = 0.15$, the voltage transfer function is found to be

$$G_{vDCM} = \frac{2.799\times10^4}{0.0004\,s + 2.875} \quad (9)$$

The three linearizing points are selected to represent the most typical operating conditions.

A simulation of the circuit has been developed in PLECS. For all three scenarios, d is perturbed with a signal which has an amplitude of 0.001 and an initial period of 0.01s to enable the circuit to reach steady-state conditions before starting the frequency sweep analysis in PLECS. From Fig. 8 it can be seen that the modelling for $\overline{|i_L|}$ is accurate up to 10 kHz, where the gain from the circuit starts to decrease in both the CCM and DCM cases. The response is good enough to have the controller designed with a 5 kHz bandwidth, which is suitable for the application. Fig. 9 proves the accuracy of the modelling work on v_{out} to d and the transfer function is suitable to use for designing a controller with 1.5 kHz bandwidth.

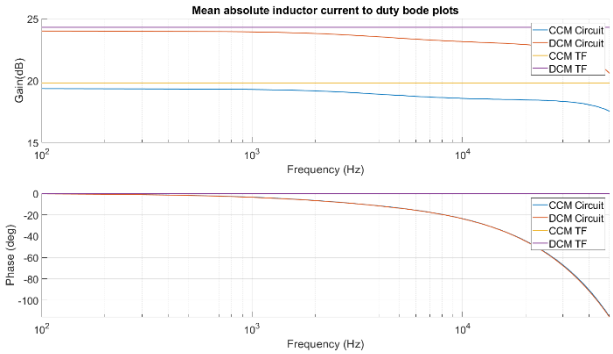

Fig. 8 Bode plots comparison for $\overline{|i_L|}$ to d under both CCM and DCM modes

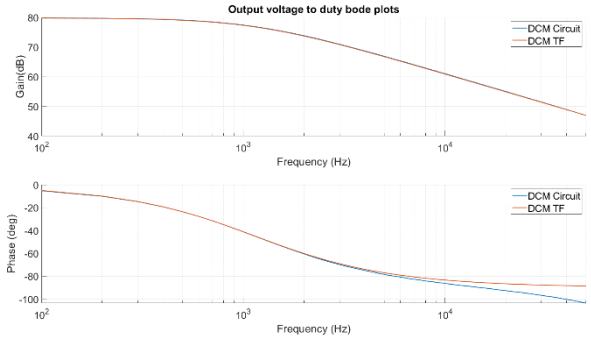

Fig. 9: Bode plots comparison for v_{out} to d under DCM mode

IV. Current and Voltage Controller Design and Validation

The control design block diagram is shown below in Fig. 10. The switch element in the middle of the diagram determines the current state of the converter and decides whether the current or voltage controller should be implemented.

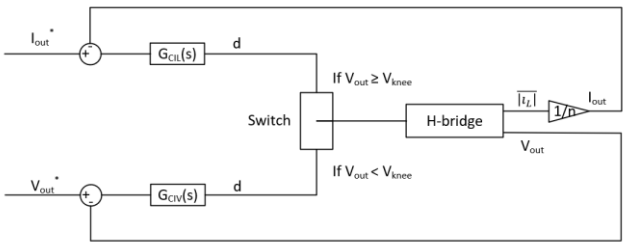

Fig. 10: Control block diagram

As the $|i_L|$ to d transfer functions are only gains, an integral controller is sufficient for effective control. If only one current controller is used, it can avoid the oscillation that may occur at the transition point when changing controller gains around the CCM/DCM boundary. Since the circuit operates under the DCM mode most of the time, a DCM controller with a natural frequency of 5 kHz is designed and used in the simulation. This control bandwidth is achieved because of the high switching frequency of the converter. A high-speed control is likely to respond more quickly to any undesirable operating conditions, such as arcing in the RF tube and ripple from uncontrolled rectifier input, meaning that its lifetime can potentially be extended [13].

Overshoot on the applied voltage to the tube may result in tube stress but can also result in a significant change in tube current when it is conducting. A 0.22% voltage overshoot can result in a 10% change in tube current, which will result in a significant variation in output power. A PI controller is adopted for voltage control, with the natural frequency of 1500 Hz and damping ratio $\xi = 1$. This high damping ratio aims to avoid the aforementioned issue. To increase the recovery speed from integrator saturation, an integrator anti-windup system is designed and implemented in the voltage control loop [18].

The combined control method is verified in a PLECS simulation, and the results are shown in the figures below. In Fig. 11, the output current reference is initially raised to 0.125 A and then increases to 1.08 A in steps of 0.192 A, before reducing to 0.125 A in steps of 0.48 A and 0.475 A. Although the Magnetron is capable of operating at currents below 0.125 A, it is selected as the minimum economic power point as any output power lower than that results in low tube efficiency. The highest reference current is selected because the Magnetron can output the maximum possible power with a 1.08 A anode current. Each phase of the converter can be individually controlled to make sure the best phase cancellation can be achieved, even in the presence of unbalanced circuit parameters (such as the ac link inductor). To avoid the large voltage error at the start, the voltage reference ramped up from 0 V to the required knee voltage in 0.00064 s. At 0.001283 s the converter is changed from voltage control to current. The current controller output value is set to be the same as the voltage controller output when the knee voltage is almost reached for a smooth changeover. The output current can be controlled accurately and rapidly as designed.

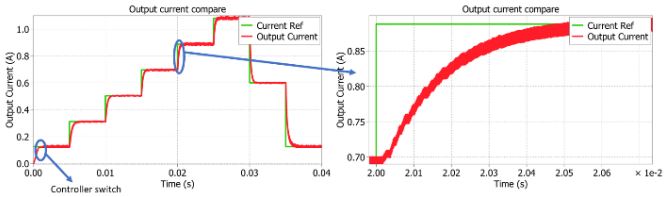

Fig. 11 Combined controller test result

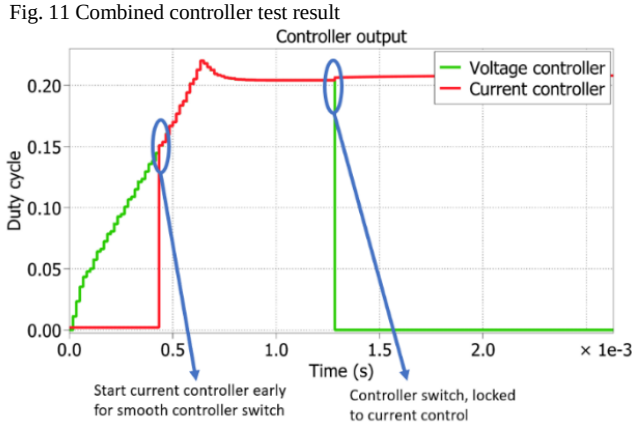

Fig. 12: Controller output during the transition

The circuit behaviour is also as expected and is analysed under both CCM and DCM modes. The waveforms are shown in Fig. 13 and Fig. 14.

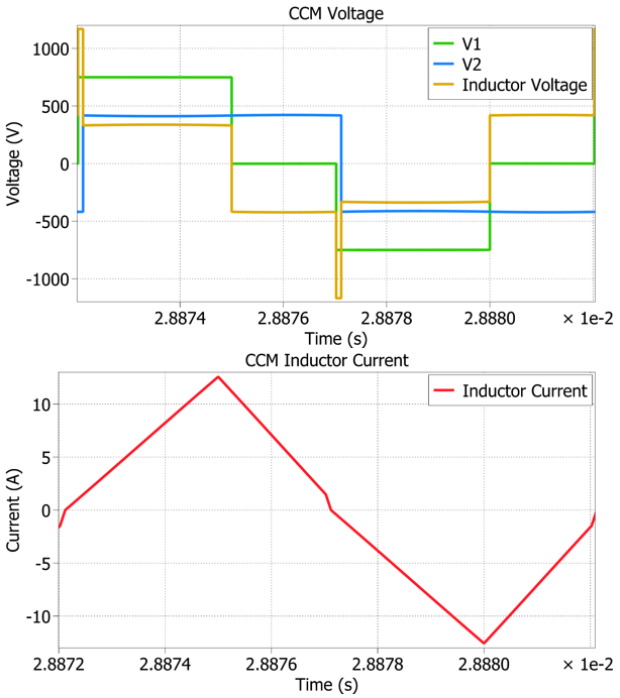

Fig. 13: CCM waveforms

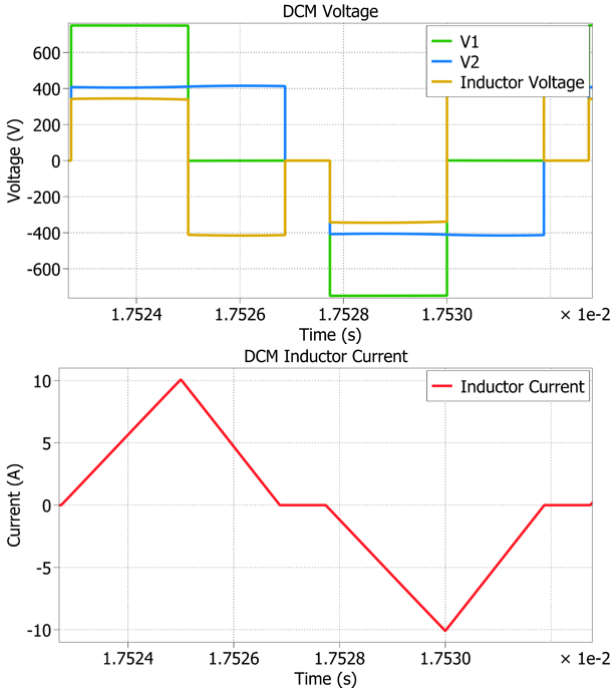

Fig. 14: DCM waveforms

V. Transformer Design

As a result of the required high operational frequency, the transformer for the SAB needs to be carefully designed. For a three-phase interleaved converter, each transformer needs to step up the voltage to 2.5 kV at 100 kHz and deliver 2.7 kW of power. Considering the future expansion of extending the converter for 100 kW magnetrons, a multi-objective optimization is carried out in MATLAB to find the optimum transformer design. The flowchart for such a process is shown in Fig. 15 with one of the optimisation results shown in Fig. 16. The design and core specifications can include transformer type, voltage and current of the windings, operating frequency, turns ratio, material characteristics and core geometries. The optimising variables can include primary turns, individual strand size of the Litz wires and current density in windings. The discontinuous curve is due to primary turns and the number of layers is rounded to the ceiling integer to avoid impractical solutions. The practical issues are considered as well. Litz wires are selected from a dataset which is possible to purchase off the shelf [19]. This can be relaxed for better design flexibility. Sudden increases in loss are the result of layer number change, which increases the ac resistance because of the proximity effect [20]. A range of nanocrystalline toroid cores are studied, and a selection of results is shown in Table 2. It can be seen that with the nanocrystalline toroid core, a small toroid core with 64g can achieve an efficiency of over 99%.

In the flowchart, subscript 1 and 2 correspond to the primary and secondary winding; J is the current density; N is the number of turns, m is the number of layers, B is flux density, R_{ac} is the ac resistance and P_{core}, P_{cu} and P_{tot} are core, copper and total losses respectively.

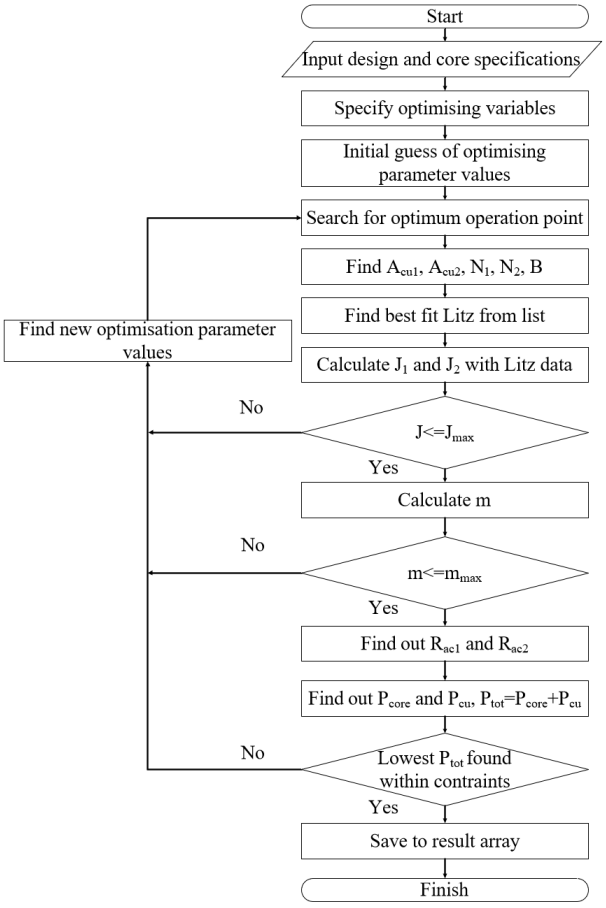

Fig. 15: Transformer optimisation flowchart

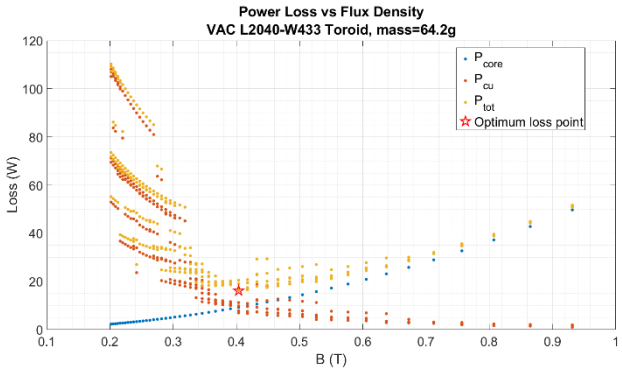

Fig. 16: Example optimisation result with VAC L2030W37604 toroid core

Table 2: Selection of the transformer optimisation results

	$B(T)$	P_{tot} (W)	N_1	$layers$	$mass$ (g)
W376	0.761	23.977	24	6	33
W433	0.404	16.127	30	5	64
W434	0.280	13.923	49	4	79

VI. Conclusions

In this paper, the design of a three-phase interleaved SAB converter which has been developed for use as a high-power industrial Magnetron power supply has been presented. An emulator for the Magnetron is shown for simulating the voltage and current characteristics of the tube. Modelling and control of the converter with a

Magnetron load are achieved and validated using simulations, with good results obtained under all conditions. A transformer optimisation algorithm has been proposed and satisfactory results collected.

REFERENCES

[1] F. Perera, "Pollution from Fossil-Fuel Combustion is the Leading Environmental Threat to Global Pediatric Health and Equity: Solutions Exist," *International Journal of Environmental Research and Public Health*, vol. 15, no. 1, p. 16, 2017.

[2] O. Roelofsen, K. Somers, E. Speelman and M. Witteveen, "Plugging in: What electrification can do for industry," 28 May 2020. [Online]. Available: https://www.mckinsey.com/industries/electric-power-and-natural-gas/our-insights/plugging-in-what-electrification-can-do-for-industry#. [Accessed 20 July 2021].

[3] R. J. Meredith, Engineers' handbook of industrial microwave heating, London: Institution of Electrical Engineers, 2007.

[4] S.-R. Jang, S.-H. Ahn, H.-J. Ryoo and J.-S. Kim, "Design of High-efficiency Soft-switching Converters for High-power Microwave Generation," *Journal of the Korean Physical Society*, vol. 59, no. 6, p. 3688~3693, 2011.

[5] J. Robinson, S. Kingman, C. Snape, M. Bradley, S. Bradshaw, D. Thomas and P. Page, "Microwave Treatment of Oil-Contaminated Drill Cuttings at Pilot Scale," *SPE Drilling & Completion*, vol. 24, no. 3, pp. 430-435, 2009.

[6] D. Siemaszko, L. de Mallac, S. Pittet and D. Aguglia, "Modular resonant converter for 25kV-8A power supply: Design, implementation and real time simulation," in *2014 16th European Conference on Power Electronics and Applications*, Lappeenranta, 2014.

[7] N. A. Abodhir, A. J. Watson, C. Ji and J. C. Clare, "Design and implementation of magnetron power supply and emulator," in *2016 18th European Conference on Power Electronics and Applications (EPE'16 ECCE Europe)*, Karlsruhe, 2016.

[8] R. W. Erickson and D. Maksimovic, Fundamentals of Power Electronics, Springer US, 2001.

[9] S. Mao, P. Jelena and J. A. Ferreira, "Analysis of the Transformer Modularization for High Frequency Isolated High Voltage Generator with the Silicon Carbide Devices," in *2020 22nd European Conference on Power Electronics and Applications (EPE'20 ECCE Europe)*, Lyon, 2020.

[10] D. Rothmund, T. Guillod, D. Bortis and J. W. Kolar, "99% Efficient 10 kV SiC-Based 7 kV/400 V DC Transformer for Future Data Centers," *IEEE JOURNAL OF EMERGING AND SELECTED TOPICS IN POWER ELECTRONICS*, vol. 7, no. 2, pp. 753-767, 2019.

[11] Sairem, "6000 W, 2450 MHz Microwave Generator GMP 60K," 2017. [Online]. Available: https://www.aetjapan.com/hardware/temp/Sairem/GMP_60K_EN.pdf. [Accessed 8 3 2023].

[12] A. Ioinovici, Power electronics and energy conversion systems. Volume 1, Fundamentals and hard-switching converters, Chichester: John Wiley & Sons, 2013.

[13] A. S. Gilmour, Klystrons, Traveling Wave Tubes, Magnetrons, Crossed-Field Amplifiers, and Gyrotrons, Artech, 2011.

[14] Y. Zhou, Y. Zhang, H. Zhu and Y. Yang, "Study of the Influence of Power Supply Ripple on Magnetron's Output Spectrum," *IEEE TRANSACTIONS ON ELECTRON DEVICES*, vol. 68, no. 9, pp. 4698-4704, 2021.

[15] J. Li, H. Wu, T. Xu and P. Lin, "Design of High Performance Magnetron Power Supply on the Basis of PWM Power Control," *Journal of Physics: Conference Series*, vol. 1601, 2020.

[16] J. Chen, Y. Tang, Y. Shen, Wang, Zhenzhen and C. Hu, "The Design of Microwave Heating Magnetron Power Supply," *Electronic Design Engineering*, vol. 23, no. 24, pp. 80-83, 2015.

[17] G. D. Demetriades, "On Small-Signal Analysis and Control of the Single and the Dual Active Bridge Topologies," Royal Institute of Technology, Stockholm, 2005.

[18] G. C. Goodwin, S. F. Graebe and M. E. Salgado, Control System Design, London : Prentice Hall, 2001.

[19] OSCO, "Litz Wire Stock," OSCO, 8 March 2023. [Online]. Available: https://www.osco.uk.com/shop/litz-wire. [Accessed 8 March 2023].

[20] W. G. Hurley and W. H. Wolfle, Transformers And Inductors For Power Electronics, Chichester: John Wiley & Sons Ltd, 2013.